

Studying the interstellar medium of H II/BCD galaxies using IFU spectroscopy

Patricio Lagos and Polychronis Papaderos

Centro de Astrofísica da Universidade do Porto
Rua das Estrelas, 4150-762 Porto, Portugal
plagos@astro.up.pt; papaderos@astro.up.pt

August 7, 2018

Abstract

We review the results from our studies, and previous published work, on the spatially resolved physical properties of a sample of H II/BCD galaxies, as obtained mainly from integral-field unit spectroscopy with Gemini/GMOS and VLT/VIMOS. We confirm that, within observational uncertainties, our sample galaxies show nearly spatially constant chemical abundances, similar to other low-mass starburst galaxies. They also show He II $\lambda 4686$ emission with properties being suggestive of a mix of excitation sources, with Wolf-Rayet stars being excluded as the primary one. Finally, in this contribution we include a list of all H II/BCD galaxies studied thus far with integral-field unit spectroscopy.

1 Introduction

The concept of *compact galaxies* was introduced by Zwicky [69], who has described them as “galaxies barely distinguishable from stars” on the Palomar Sky Survey plates. The term blue compact dwarf (BCD) galaxies [62] identify those objects that show low luminosity, small linear dimensions, strong emission lines superposed on a blue continuum, and spectral properties that indicate low chemical abundances. BCDs form a subset of H II galaxies, a large number of which have been identified on objective prism surveys by [19], [70], [46] and [56] by the presence of strong emission lines, similar to Giant H II regions (GH II Rs) in our galaxy. Here, we will refer to H II/BCD galaxies as objects with a metallicity $7.0 \leq 12 + \log(O/H) \leq 8.4$ (e.g., [33]), low luminosity ($M_B \gtrsim -18$) and gas-rich objects (e.g., [13]) undergoing vigorous starburst activity in a relatively small physical size ($\lesssim 1$ Kpc). The star-forming component, in these objects, typically contains multiple knots of star-formation with unresolved ensembles of young star clusters (e.g., [34], [37]). The hypothesis of these systems being young, forming their first generation of stars has been discarded by the detection of an evolved underlying stellar host with an age > 1 Gyr, in the majority of the nearby H II/BCD population (e.g., [51],[60]). Figure 1 shows the optical spectrum of the galaxy Tol 2146-391 obtained using integral field unit (IFU) observations with Gemini/GMOS. In this figure we label the most important emission lines used in our studies, in particular, the strong Balmer hydrogen recombination lines and collisionally excited emission

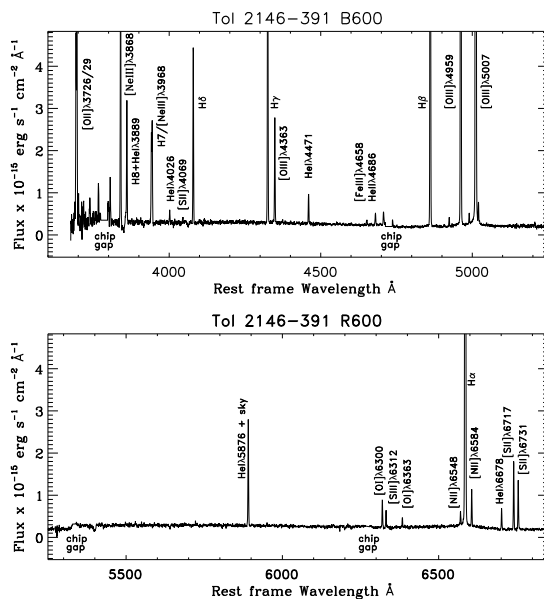


Figure 1: Integrated spectra of the H II/BCD galaxy Tol 2146-391. Top panel: blue spectrum (grating B600). Bottom panel: red spectrum (grating R600).

lines, such as [O II] $\lambda\lambda 3726, 3729$, [O III] $\lambda 4363$, [O III] $\lambda 5007$, [S II] $\lambda\lambda 6717, 6731$, [N II] $\lambda 6584$, which have been used for the determination of physical conditions (e.g., electron temperature and density) and chemical abundances (e.g., oxygen, nitrogen, etc). We also detect in some of our galaxies the high-ionization emission line He II $\lambda 4686$.

Although progress has been made in this field, important unsolved questions remain with regard to the mode of star formation (e.g., quasi-continuous vs fluctuating), and the triggering mechanism of ongoing starburst activity in H II/BCDs. It has been suggested [37] that the cluster formation efficiency is lower in compact H II/BCD galaxies than the one found in more luminous galaxies. These luminous systems generally show an irregular outer shape and kinematical signatures of merging in their interstellar medium (ISM). In some cases, the formation of star cluster complexes occurs coevally [37], whereas in others star formation occurs in a propagating manner [52, 54]. In any case, the mechanism which may trigger the current star-formation in these galaxies is not well understood; in particular the relative importance of intrinsic and environmental properties remains a subject of investigation.

Another important issue is the chemical and kinematical imprints of star cluster formation and evolution on the spatially resolved properties of the ISM in H II/BCD galaxies. As a natural consequence of star formation driven feedback, the newly synthesized elements will be dispersed and mixed across the ISM via hydrodynamic mechanisms (e.g., [61]), leading to *chemical homogeneity in the oxygen abundance* [30, 32] of H II/BCD galaxies (e.g., [35] and references therein). The nitrogen-to-oxygen ratio N/O has also been found to be rather constant ($\log(N/O) \simeq -1.6$; [12, 1, 20]) at low metallicity ($12 + \log(O/H) \leq 7.6$), suggesting primary production by massive stars [20] as the main contribution to nitrogen enrichment at those very low metallicities. A

small fraction of H II/BCD galaxies fall in this very-low metallicity regime [50] and are commonly referred to as extremely metal poor (XMP) galaxies or XMP BCDs. These galaxies are the best nearby candidates for cosmologically young objects, as various arguments imply that they have formed most of their stellar mass in the past 1–3 Gyr [53]. At intermediate metallicity ($7.6 \leq 12 + \log(\text{O}/\text{H}) \leq 8.3$) the large observed spread in N/O has been attributed mainly to the loss of heavy elements via galactic winds [66], and/or to the delayed release of nitrogen by intermediate and/or massive stars and oxygen by massive stars [12, 15]. However, the delayed-release scenario cannot explain the presence of some H II/BCD galaxies with a high N/O ratio at low metallicities. The most plausible explanation for the high N/O ratio observed in these objects is the chemical pollution of the ISM by nitrogen released by massive Wolf-Rayet (WR) stars as is, apparently, the case of the well-studied BCD NGC 5253 [64, 31, 42, 65]. Finally, at higher metallicities ($12 + \log(\text{O}/\text{H}) \geq 8.3$) the N/O ratio clearly increases with increasing oxygen abundance and the nitrogen content is mainly due to secondary production by intermediate-mass stars.

So far, an increasing number of H II/BCD galaxies has been studied with IFU spectroscopy (see Table 1 where we provide an overview of the literature) with main focus on the spatial properties of the ISM. Recently, we have started a program investigating with IFU spectroscopy the physical conditions in the ISM of the most compact H II/BCD galaxies, laying special emphasis on the extinction patterns, emission line ratios, oxygen and nitrogen abundances, kinematics and the relation on the intrinsic properties of star formation as well as possible evolutionary effects [35, 39]. To this end, we observed a sample of H II/BCD galaxies using the GMOS-IFU on Gemini South and North and, more recently, with VLT/VIMOS. The GMOS-IFU observations were performed using the gratings B600 and R600 in one slit mode, covering a total spectral range from ~ 3000 to ~ 7230 Å. This observational setup provides a pattern of 500 hexagonal elements with a projected diameter of $0''.2$, covering a total $3''.5 \times 5''$ field of view (FoV). The VIMOS-IFU observations were obtained using the gratings HR_blue and HR_orange covering a spectral range from ~ 3710 to ~ 7700 Å. Our data yield a scale on the sky of $0''.33$ per fiber, and cover a FoV of $13'' \times 13''$. In Figure 2 we show the g-band acquisition image of the XMP BCD galaxy HS2236+1344, in which we indicated the total field of view of $4'' \times 8''$ and the H α map of the galaxy obtained from the composition of two different pointings with GMOS-IFU. In Figure 3 we show the H α emission line map of the galaxies UM 461 and Tol 65 obtained using VIMOS-IFU. Table 2 lists the general parameters of our sample of galaxies.

This contribution is organized as follows: the metallicity content and the spatial distribution of the ISM in our sample galaxies are described in Section 2, and in Section 3 we discuss the high-ionization emission line He II $\lambda 4686$ and its relationship to the properties of the ISM. Finally, in Section 4, we summarize our results and conclusions.

2 The metal content in the ISM of H II/BCD galaxies

Using the reddening corrected emission line intensities of the spectra of each one of the spaxels we can derive the physical conditions (electron temperature and density) and the chemical abundances (O and N) across the ISM of the galaxies. We calculate oxygen abundances in regions where the [OIII] $\lambda 4363$ emission line has been detected assuming $\text{O}/\text{H} = \text{O}^+/\text{H}^+ + \text{O}^{++}/\text{H}^+$, while nitrogen abundances are obtained assuming $\text{N}/\text{H} = \text{ICF}(\text{N}) \times \text{N}^+/\text{H}^+$, with ICF(N) denoting the ionization correction factor $(\text{O}^+ + \text{O}^{+2})/\text{O}^+$. For the sake of illustration, in Figure 4 we show the spatial distribution

Table 1: H II/BCD galaxies with published IFU observations. The list could be incomplete and does not include Fabry-Perot observations. Redshift distances obtained from NED assuming $H_0 = 73 \text{ km s}^{-1} \text{ Mpc}^{-1}$. M_B computed from the tabulated values of m_B obtained from HyperLeda.

Name	Coordinates (J2000)		Distance (Mpc)	M_B (mag)	Reference	Instrument
IC 10	00:20:17.3	+59:18:14	0.8	-12.73	[44]	PMAS
Haro 11	00:36:52.7	-33:33:17	84.6	-20.30	[27]	FLAMES
Tol 0104-388	01:07:02.2	-38:31:51	91.6	...	[38, 39]	GMOS-IFU
Mrk 996	01:27:35.5	-06:19:36	22.2	-16.56	[24]	VIMOS-IFU
HS0128+2832	01:31:21.3	+28:48:12	66.3	...	[55]	PMAS
UM 408	02:11:23.4	+02:20:30	49.3	-15.76	[35, 36]	GMOS-IFU
UM 420	02:20:54.5	+00:33:24	240.1	-21.19	[25]	VIMOS-IFU
Mrk 370	02:40:29.0	+19:17:50	10.8	-16.40	[14]	INTEGRAL
SBS 0335-052	03:37:44.0	-05:02:40	55.6	-16.77	[68, 22]	SINFONI, FLAMES
IIZw 33	05:10:48.1	-02:40:54	38.8	-18.45	[8]	VIRUS-P
IIZw 40	05:55:42.6	+03:23:32	10.8	-16.69	[67, 3]	SINFONI, GMOS-IFU
Haro 1	07:36:56.7	+35:14:31	51.9	-21.02	[8]	VIRUS-P
He 2-10	08:36:15.1	-26:24:34	12.0	-17.93	[45, 9]	FLAMES, SINFONI
HS0837+4717	08:40:29.9	+47:07:10	172.4	-18.15	[55]	PMAS
Mrk 1418	09:40:27.0	+48:20:15	10.6	-16.27	[6]	PMAS
Mrk 407	09:47:47.6	+39:05:03	21.8	-16.50	[7]	PMAS
Mrk 409	09:49:41.2	+32:13:16	21.2	-17.11	[5]	PMAS
Tol 1004-296	10:06:33.4	-29:56:05	15.3	-17.56	[68]	SINFONI
Mrk 32	10:27:02.0	+56:16:14	11.4	-14.20	[7]	PMAS
Mrk 35	10:45:22.4	+55:57:37	12.9	-17.33	[14]	INTEGRAL
Mrk 178	11:33:28.9	+49:14:14	3.4	-13.25	[29]	INTEGRAL
UM 448	11:42:12.4	+00:20:03	76.3	-19.93	[26]	FLAMES
Mrk 750	11:50:02.7	+15:01:23	10.3	-14.30	[7]	PMAS
UM 462	11:52:37.2	-02:28:10	14.5	-16.20	[25]	VIMOS-IFU
Mrk 206	12:24:17.0	+67:26:24	18.0	-15.90	[7]	PMAS
NGC 4670	12:45:17.1	+27:07:31	14.7	-17.68	[8]	VIRUS-P
NGC 5253	13:39:55.9	-31:38:24	5.6	-17.68	[9, 47, 48, 65]	SINFONI, FLAMES, GMOS-IFU
Tol 1434+032	14:37:08.9	+03:02:50	23.4	-14.94	[7]	PMAS
Mrk 475	14:39:05.4	+36:48:22	8.0	-13.10	[7]	PMAS
IIZw 70	14:50:56.5	+35:34:18	16.2	-16.28	[28]	PMAS
I Zw 123	15:37:04.2	+55:15:48	9.1	-14.35	[7]	PMAS
Mrk 297	16:05:13.0	+20:32:32	65.0	-20.60	[14]	INTEGRAL
I Zw 159	16:35:21.0	+52:12:52	37.0	-17.19	[7]	PMAS
Tol 2146-391	21:49:48.2	-38:54:09	120.7	...	[38, 39]	GMOS-IFU
HS2236+1344	22:38:31.1	+14:00:30	84.5	...	[40]	GMOS-IFU
Mrk 314	23:02:59.2	+16:36:19	28.5	-18.20	[14, 8]	INTEGRAL, VIRUS-P
III Zw 102	23:20:30.1	+17:13:32	22.4	-18.81	[14, 8]	INTEGRAL, VIRUS-P
Mrk 930	23:31:58.3	+28:56:50	75.2	...	[55]	PMAS

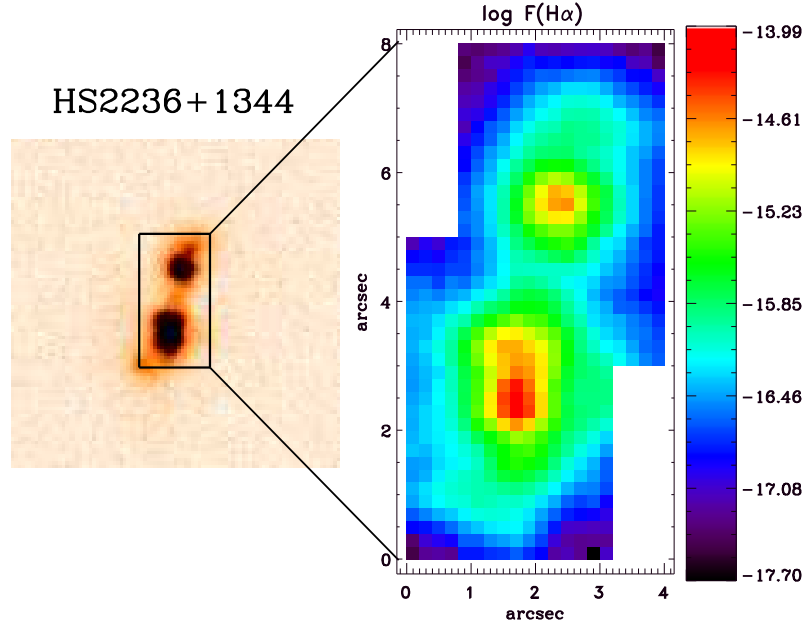


Figure 2: GMOS-IFU observation of the XMP galaxy HS2236+1344. Left: g-band acquisition image of the galaxy. The rectangle indicates the total field of view of 4''x8'' obtained from the composition of two different pointings with GMOS. Right: H α map of the galaxy. $\log F(\text{H}\alpha)$ in units of $\text{ergs cm}^{-2} \text{s}^{-1}$. Further details will be presented in a forthcoming paper [40].

Table 2: General parameters of our studied galaxies.

Name	Coordinates ^a (J2000)		D (Mpc) ^a	M_B^b (mag)	12+log(O/H)	Instrument
Tol 0104-388	01:07:02.2	-38:31:51	91.6	...	8.02 ^[39]	GMOS-IFU
UM 408	02:11:23.4	+02:20:30	49.3	-15.76	7.87 ^[35]	GMOS-IFU
Mrk 600	02:51:04.6	+04:27:14	13.8	-15.38	7.88 ^[18]	VIMOS-IFU
UM 461	11:51:33.3	-02:22:22	14.2	-14.36	7.72 ^[49]	VIMOS-IFU
Tol 65	12:25:46.9	-36:14:01	38.5	-15.44	7.53-7.56 ^[18]	VIMOS-IFU
Tol 2146-391	21:49:48.2	-38:54:09	120.7	...	7.82 ^[39]	GMOS-IFU
HS2236+1344	22:38:31.1	+14:00:30	84.5	...	7.55 ^[40]	GMOS-IFU

^aObtained from NED

^bObtained from HyperLeda

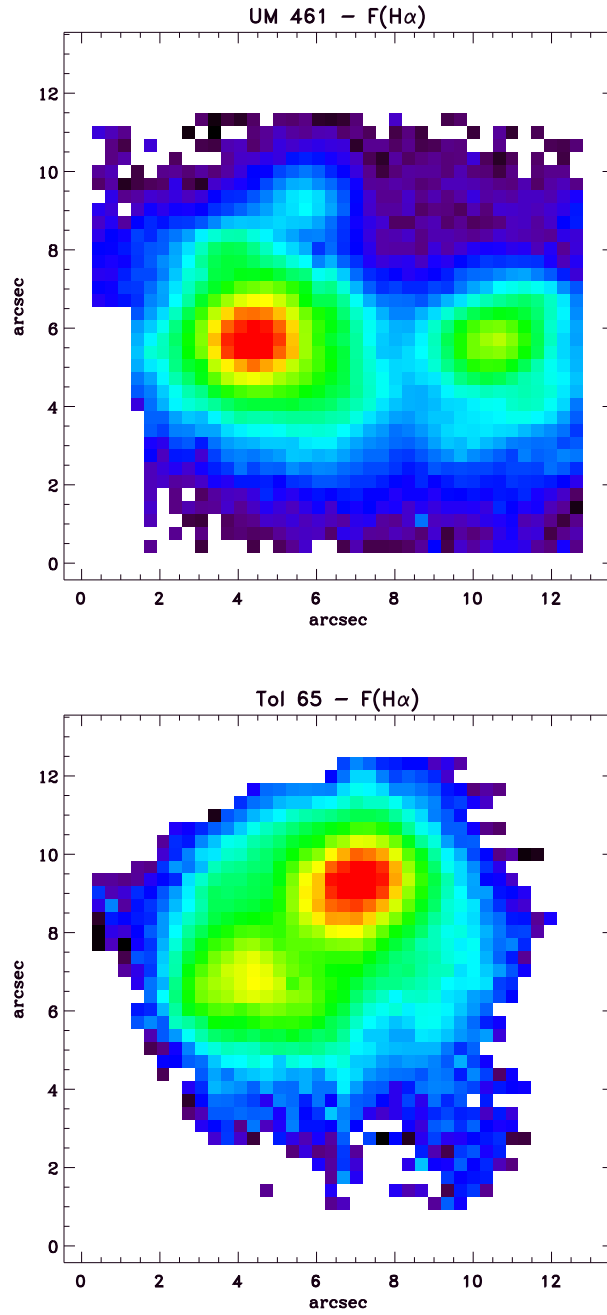


Figure 3: VIMOS-IFU $H\alpha$ emission line map of the XMP BCD galaxies UM 461 (Top panel) and Tol 65 (Bottom panel). North is to the top and East to the left. Further details will be presented in a forthcoming paper.

of $12+\log(\text{O}/\text{H})$ in the GMOS-IFU FoV of the galaxy Tol 2146-391. We can see in this figure that, despite a slight depression in the inner part of the galaxy, the oxygen abundance appears to be uniform across the galaxy (see Figure 18 in [39]). In [36] we compare the spatial distribution of $12+\log(\text{O}/\text{H})$, found in [35], with the position of the star cluster/complexes detected in the galaxy UM 408 by [37] using high resolution near-IR K_p -band images. We found that the variation of the observed data points (see Figure 9 in [35] and Figure 1 in [36]) may not be statistically significant, indicating that these regions have identical chemical properties within the errors. It is interesting to note that we observed a marginal gradient of decreasing abundance from the center outward in UM 408, indicating that the highest abundance values are found near the peak of $\text{H}\alpha$ emission and extinction $c(\text{H}\beta)$, and coincident with the position of the brightest star cluster/complex [37]. In any case, the absence of chemical overabundances in the ISM of UM 408, Tol 2146-391, Tol 0104-388 and HS2236+1344 and in the dwarf galaxies studied in the literature (e.g., [58, 30, 32, 41, 10, 2]) indicates that the population of young star clusters is not producing localized oxygen overabundances. The most likely explanation for this is that metals formed in the current star-formation episode reside in a hot gas phase ($T\sim 10^7$ K; [61]); thus, they are not observable in optical wavelengths. Whereas metals from previous star-formation events are well mixed and homogeneously distributed through the whole galaxy. In Tol 2146-391, the $12+\log(\text{N}/\text{H})$ radial distribution shows a slight decrease with radius. This would argue in favor of heavy elements being produced in a previous burst of star-formation and dispersed within the ISM by starburst-driven super-shells [39], while the depressed central region could be attributed to radial inflow of relatively low metallicity gas from large radii to the center, thus diluting the abundance of the gas in the nuclear region.

Regarding the integrated properties of the galaxies, [23], [4] and [43] suggest that there is a dependence between N/O and the $\text{EW}(\text{H}\beta)$, in the sense of an increasing N/O ratio with decreasing $\text{EW}(\text{H}\beta)$. Izotov et al. [23] argue that this trend is naturally explained by nitrogen ejection from WR stars. In the following analysis, we mainly concentrate on the spatially resolved physical properties of the ISM in individual galaxies and their possible relation to the star formation process (e.g., the star formation history, burst parameter, WR star content). In Figure 5 (see [39]) we show the $\log(\text{N}/\text{O})$ versus $\text{EW}(\text{H}\beta)$ and $12+\log(\text{O}/\text{H})$ versus $\log(\text{N}/\text{O})$ for all spaxels of the galaxies Tol 0104-388 and Tol 2146-391. From that figure, it can be seen that the $\text{EW}(\text{H}\beta)$ values are rather constant, with a very small variation of equivalent widths as the N/O ratio increases. A comparison of $\log(\text{N}/\text{O})$ versus $12+\log(\text{O}/\text{H})$ in Tol 2146-391 (Figure 3b) reveals that the $\log(\text{N}/\text{O})$ values increase with the $12+\log(\text{O}/\text{H})$. This data point distribution has similar patterns to those found in $\text{H}\text{II}/\text{BCD}$ galaxies by [20] of increasing N/O ratios with respect to the oxygen abundance. The inner region of Tol 2146-391 (near the peak of $\text{H}\alpha$) presents N/O ratios which are larger than those expected by pure primary production of nitrogen. This might be a signature of time delay between the release of oxygen and nitrogen [32], or gas infall or outflow. In any case, for the metallicity of Tol 2146-391 purely secondary nitrogen enrichment appears implausible. In the case of HS2236+1433, we reported in [40] evidence for a high N/O ratio in one of the three $\text{GH}\text{II}Rs$ of the galaxy. But again, the spatial distribution of these abundances, at large scales, lead us to consider that oxygen and hydrogen are well mixed and homogeneously distributed over the ISM of the galaxy.

In summary, the results obtained in our studies suggest that the chemical properties (O , N and N/O) across $\text{H}\text{II}/\text{BCD}$ galaxies are fairly uniform, although a slight gradient of O and N are observed in the ISM of UM 408 and Tol 2146-391, respectively. We suggest that global hydro-dynamical processes, such as starburst-driven super-shells

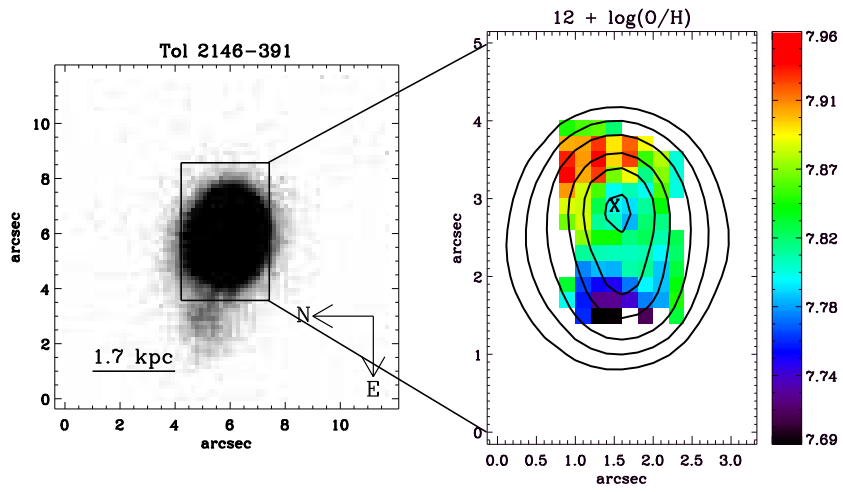


Figure 4: Spatial distribution of oxygen abundances in the galaxy Tol 2146-391. Left: g-band acquisition image of the galaxy. The rectangle indicates the FoV of $3''.5 \times 5''$ covered by our GMOS-IFU observation. Right: $12 + \log(\text{O}/\text{H})$ spatial distribution. The isocontours display the $\text{H}\alpha$ emission. The maximum $\text{H}\alpha$ emission is indicated in the maps by an X symbol. We only considered spaxels with signal to noise ratio (S/N) > 3 in the $[\text{OIII}] \lambda 4363$ line. More details in [39].

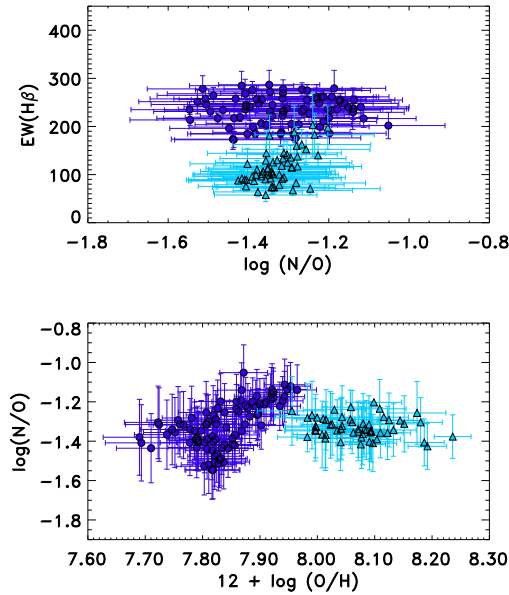


Figure 5: Top panel: $\log(N/O)$ ratio versus $EW(H\beta)$. Bottom panel: $12 + \log(O/H)$ ratio versus $\log(N/O)$. Triangles correspond to the data points of Tol 0104-388 and circles corresponds with the data points of Tol 2146-391. More details in [39].

or/and inflow of gas might be governing the transport and mixing of metals across these galaxies, keeping the N/O ratio constant through the ISM at large scales [55, 39].

3 The high ionization emission line He II $\lambda 4686$

The origin of high-ionization emission lines, such as [Ne V] $\lambda 3426$, [Fe V] $\lambda 4227$ and He II $\lambda 4686$ in starburst and H II/BCD galaxies has been a subject of study in the last years, given that photoionization models of H II regions generally fail to reproduce the observed intensities of these lines (see, e.g., [21]). Several mechanisms for producing hard ionizing radiation have been proposed in the literature, such as WR stars [57], primordial (zero-metallicity) stars, high-mass X-ray binaries (HMXB; [16]), radiative shocks [11] and O stars at low metallicity [4]. In [39] and [40] we studied with GMOS-IFU the spatial distribution of He II $\lambda 4686$ in the compact H II galaxies Tol 0104-388 and Tol 2146-391, and in the XMP BCD galaxy HS 2236+1344, respectively, in order to gain insights into the nature of their hard ionization radiation and its possible dependence on the properties of the ISM [16, 21].

Based on a spaxel-by-spaxel analysis, instead of the integrated properties of the galaxies (see Figure 15 in [39]), our results indicate that the spatial distribution of He II $\lambda 4686$ relative to H β does not depend on the $EW(H\beta)$, oxygen abundance or $\log(N/O)$. In particular, the oxygen abundance appears to be constant through the whole extent of our sample galaxies, as already is observed in other H II/BCD galaxies (e.g., [35]; and references therein). The opposite trend is found if we consider the integrated spectra of galaxies, in the sense that this emission line is stronger in galaxies at low metallicity

[23]. The lack of a relationship between the hardness of the ionizing radiation and the $EW(H\beta)$, or age, [63] suggests that the presence of high-ionization lines, in particular $He\ II\ \lambda 4686$, is not due to a single excitation mechanism. For instance, in [17], it was found for a sample of galaxies, with detected and non-detected WR features, the same dependence of $I(He\ II\ \lambda 4686)/I(H\beta)$ on the $EW(H\beta)$. This indicates that WR stars are not the sole origin of $He\ II\ \lambda 4686$ in star-forming regions (see also [59]). In galaxies with detected WR stars, the $He\ II\ \lambda 4686$ commonly appears to not be coincident with the location of the WR bumps (e.g., Mrk 178) and these stellar features are not always seen when nebular $He\ II$ is observed (e.g., Tol 2146-391, HS2236+1344, Tol 65). The spatial offset between WR stars and $He\ II\ \lambda 4686$, in Mrk 178, is interpreted by [29] as an effect of the mechanical energy injected by WR star winds, so WR stars are not ruled out as the main source of the observed $He\ II\ \lambda 4686$ in that galaxy. An examination of individual spaxels in our data cubes, and also in the integrated spectra of our sample galaxies (e.g., Figure 1 in this contribution), does not reveal any clear stellar WR features. In the case of the XMP BCD galaxy HS 2236+1344, we detected the $He\ II\ \lambda 4686$ emission line in only one of the GH Π Rs of the galaxy (the brightest one). In this galaxy, the $He\ II\ \lambda 4686$ line appears to be excited through point sources within a compact volume which, interestingly, does not coincide with the position where a high N/O abundance ratio has been observed. We discuss, in [40], the possibility that the $He\ II\ \lambda 4686$ emission line, in HS2236+1344, is associated with WR stars, high-mass X-ray binaries (HMXBs), O stars at low metallicities, and/or a low-luminosity Active Galactic Nucleus. However, since clear WR features have not been detected in that galaxy, WR stars are excluded as the primary excitation source of $He\ II\ \lambda 4686$ emission.

4 Conclusions

As far as the spatial distribution of oxygen abundances is concerned, we did not detect localized overabundances in any of our sample galaxies. However, we find evidence for a marginal negative radial abundance gradient, with the highest abundances seen at the position of the brightest star cluster complexes (peak of $H\alpha$ emission), in the H Π /BCD galaxy UM 408 at least. If real, the slight trend for an increasing $12+\log(N/H)$ abundance, in the galaxy Tol 2146-391, suggests rapid self-enrichment by the freshly produced heavy elements in the present starburst on scales of hundreds of pc, or, alternatively, metal pollution by a previous star formation episode. In any case, the oxygen and nitrogen appear to be well mixed across the ISM of H Π /BCD galaxies, suggesting efficient transport by expanding starburst-driven supershells and/or gas infall from the halo.

Our spectroscopic IFU studies suggest a mixture of compact sources as the main excitation source for localized $He\ II\ \lambda 4686$ emission in H Π /BCD galaxies, without clear WR signatures, with WR stars probably being of secondary importance. In the galaxy Tol 2146-391, we favor the idea of extended $He\ II\ \lambda 4686$ emission being primarily due to radiative shocks in the ISM.

5 Acknowledgments

P.L. is supported by a Post-Doctoral grant SFRH/BPD/72308/2010, funded by FCT (Portugal), and P.P. by Ciencia 2008 Contract, funded by FCT/MCTES (Portugal) and

POPH/FSE (EC). We are very thankful to Andrew Humphrey for their very useful suggestions which have improved the paper. We would like thank the anonymous referee for his/her comments and suggestions which substantially improved the paper. We acknowledge support by the Fundação para a Ciência e a Tecnologia (FCT) under project FCOMP-01-0124-FEDER-029170 (Reference FCT PTDC/FIS-AST/3214/2012), funded by the FEDER program. This research has made use of the NASA/IPAC Extragalactic Database (NED) which is operated by the Jet Propulsion laboratory, California Institute of technology, under contract with the National Aeronautics and Space Administration. We acknowledge the usage of the HyperLeda database (<http://leda.univ-lyon1.fr>). The data presented in this paper have been obtained through the Gemini programs GS-2004B-Q-59, GS-2005B-Q-19 and GN-2010B-Q-69, and the ESO-VLT program 090.B-0242.

References

- [1] Alloin D., Collin-Souffrin S., Joly M., & Vigroux J. M., 1979, *A&A*, 78, 200
- [2] Berg, D. A., Skillman, E. D., Marble, A. R., et al. 2012, *ApJ*, 754, 98
- [3] Bordalo, V., Plana, H., & Telles, E. 2009, *ApJ*, 696, 1668
- [4] Brinchmann J., Kunth D., & Durret F., 2008, *A&A*, 485, 657
- [5] Cairós L. M., Caon N., Papaderos P., Kehrig C., Weilbacher P., & Roth M., Zurita C., 2009, *ApJ*, 707, 1676
- [6] Cairós L. M., Caon N., Zurita C., Kehrig C., Weilbacher P., & Roth M., 2009, *A&A*, 507, 1291
- [7] Cairós L. M., Caon N., Zurita C., Kehrig C., Roth M., & Weilbacher P., 2010, *A&A*, 520, 90
- [8] Cairós, L. M., Caon, N., García Lorenzo, B., Kelz, A., Roth, M., Papaderos, P., & Streicher, O. 2012, *A&A*, 547, 24
- [9] Cresci, G., Vanzi, L., Sauvage, M., Santangelo, G., & van der Werf, P. 2010, *A&A*, 520, 82
- [10] Croxall, K. V., van Zee, L., Lee, H., et al. 2009, *ApJ*, 705, 723
- [11] Dopita M. A., & Sutherland R. S., 1996, *ApJS*, 102, 161
- [12] Edmunds M. G. & Pagel B. E. J. 1978, *MNRAS*, 185, 77
- [13] Filho, M. E., Winkel, B., Sánchez Almeida, J., Aguerri, J. A., Amorín, R., Ascáibar, Y., Elmegreen, B. G., Elmegreen, D. M., Gomes, J. M., Humphrey, A., Lagos, P., Morales-Luis, A. B., Muñoz-Tuñón, C., Papaderos, P., & Vílchez, J. M. 2013, *arXiv:1307.4899*
- [14] García-Lorenzo, B., Cairós, L. M., Caon, N., Monreal-Ibero, A., & Kehrig, C. 2008, *ApJ*, 677, 201
- [15] Garnett D. R. 1990, *ApJ*, 363, 142

- [16] Garnett D. R., Kennicutt R. C., Jr, Chu Y.-H., & Skillman E. D., 1991, *ApJ*, 373, 458
- [17] Guseva N. G., Izotov Y. I., & Thuan T. X., 2000, *ApJ*, 531, 776
- [18] Guseva, N. G., Izotov, Y. I., Stasińska, G., Fricke, K. J., Henkel, C., & Papaderos, P. 2011, *A&A*, 529, 149
- [19] Haro, G. 1956, *BOTT*, 2, 8
- [20] Izotov Y. I., & Thuan T. X. 1999, *ApJ*, 511, 639
- [21] Izotov, Y.I., K.G. Noeske, N.G. Guseva et al. 2004, *A&A*, 415, 27
- [22] Izotov Y. I., Schaerer D., Blecha A., Royer F., Guseva N. G., & North P., 2006a, *A&A*, 459, 71
- [23] Izotov Y. I., Stasińska G., Meynet G., Guseva N. G., & Thuan T. X., 2006b, *A&A*, 448, 955
- [24] James, B. L., Tsamis, Y. G., Barlow, M. J., Westmoquette, M. S., Walsh, J. R., Cuisinier, F., & Exter, K. M. 2009, *MNRAS*, 398, 2
- [25] James, B. L., Tsamis, Y. G., & Barlow, M. J. 2010, *MNRAS*, 401, 759
- [26] James, B. L., Tsamis, Y. G., Barlow, M. J., Walsh, J. R., & Westmoquette, M. S. 2013, *MNRAS*, 428, 86
- [27] James, B. L., Tsamis, Y. G., Walsh, J. R., Barlow, M. J., & Westmoquette, M. S. 2013, *MNRAS*, 430, 2097
- [28] Kehrig, C., Vílchez, J. M., Sánchez, S. F., Telles, E., Pérez-Montero, E., & Martín-Gordón, D. 2008, *A&A*, 477, 813
- [29] Kehrig, C., Pérez-Montero, E., Vílchez, J. M., Brinchmann, J., Kunth, D., García-Benito, R., Crowther, P. A., Hernández-Fernández, J., Durret, F., Contini, T., Fernández-Martín, A., James, B. L. 2013, *MNRAS*, tmp.1353
- [30] Kobulnicky, H. A. & Skillman, E. D. 1997, *ApJ*, 489, 636
- [31] Kobulnicky, Henry A., Skillman, Evan D., Roy, Jean-Rene, Walsh, J. R., & Rosa, Michael R. 1997, *ApJ*, 477, 679
- [32] Kobulnicky H. A., & Skillman E. D., 1998, *ApJ*, 497, 601
- [33] Kunth, D., & Sargent, W. L. W. 1983, *ApJ*, 273, 81
- [34] Lagos, P., Telles, E., & Melnick, J., 2007, *A&A*, 476, 89
- [35] Lagos, P., Telles, E., Muñoz-Tuñón, C., Carrasco, E. R., Cuisinier, F., & Tenorio-Tagle, G. 2009, *AJ*, 137, 5068
- [36] Lagos, P., Telles, E., & Carrasco, E. R. 2010, *IAUS*, 266, 447
- [37] Lagos P., Telles, E., Nigoche-Netro, A., & Carrasco E. R. 2011, *AJ*, 142, 162
- [38] Lagos, P. & Muñoz-Tuñón, C. 2011, *EAS*, 48, 165

- [39] Lagos P., Telles E., Nigoche-Netro A., & Carrasco E. R. 2012, MNRAS, 427, 740
- [40] Lagos, P., Papaderos, P., Gomes, J. M., Vega. L. R., & Smith, A. V. 2013, A&A, in prep.
- [41] Lee, H., Skillman, E. D., & Venn, K. A. 2006, ApJ, 642, 813
- [42] López-Sánchez, A. R., Esteban, C., García-Rojas, J., Peimbert, M., & Rodríguez, M. 2007, ApJ, 656, 168
- [43] López-Sánchez A. R., & Esteban C., 2010, A&A, 517, 85
- [44] López-Sánchez, A. R., Mesa-Delgado, A., López-Martín, L., & Esteban, C. 2011, MNRAS, 411, 2076
- [45] Marquart, T., Fathi, K., Ostlin, G., Bergvall, N., Cumming, R. J., & Amram, P. 2007, A&A, 474, 9
- [46] Markarian, B. E., *Astrofizika*, 3, 24, 1967
- [47] Monreal-Ibero, A., Vílchez, J. M., Walsh, J. R., & Muñoz-Tuñón, C. 2010, A&A, 517, 27
- [48] Monreal-Ibero, A., Walsh, J. R., & Vílchez, J. M. 2012, A&A, 544, 60
- [49] Nava, A., Casebeer, D., Henry, R. B. C., & Jevremovic, D. 2006, ApJ, 645, 1076
- [50] Kunth, D. & Östlin, G. 2000, A&ARv, 10, 1
- [51] Papaderos, P., Loose, H.-H., Thuan, T. X., & Fricke, K. J. 1996, A&AS, 120, 207
- [52] Papaderos, P., Izotov, Y.I., Fricke, K.J., Thuan, T.X., Guseva, N.G. 1998, A&A, 338, 43
- [53] Papaderos P., Izotov Y. I., Thuan T. X., Noeske K. G., Fricke K. J., Guseva N. G., & Green R. F., 2002, A&A, 393, 461
- [54] Papaderos, P., Guseva, N. G., Izotov, Y. I., & Fricke, K. J. 2008, A&A, 491, 113
- [55] Pérez-Montero, E., Vílchez, J. M., Cedrés, B., Hagele, G. F., Mollá, M., Kehrig, C., Díaz, A. I., García-Benito, R., & Martín-Gordón, D. 2011, A&A, 532, 141
- [56] Sargent, W. L. W. & Searle, L. 1970, ApJ, 162, 155
- [57] Schaerer D., 1996, ApJ, 467, 17
- [58] Skillman, E. D., Kennicutt, R. C., & Hodge, P. W. 1989, ApJ, 347, 875
- [59] Shirazi, M., & Brinchmann, J. 2012, MNRAS, 421, 1043
- [60] Telles, E., & Terlevich, R. 1997, MNRAS, 286, 183
- [61] Tenorio-Tagle, G. 1996, AJ, 111, 1641
- [62] Thuan, T.X. & Martin, G.E. 1981, ApJ, 247, 823
- [63] Thuan T. X., & Izotov Y. I., 2005, ApJS, 161, 240
- [64] Walsh, J. R. & Roy, J.-R. 1989, MNRAS, 239, 297

- [65] Westmoquette, M. S., James, B., Monreal-Ibero, A., & Walsh, J. R. 2013, A&A, 550, 88
- [66] van Zee L., Salzer J. J., & Haynes M. P., 1998, ApJ, 497, 1
- [67] Vanzi, L., Cresci, G., Telles, E., & Melnick, J. 2008, A&A, 486, 393
- [68] Vanzi, L., Cresci, G., Sauvage, M., & Thompson, R. 2011, A&A, 534, 70
- [69] Zwicky, I. F. 1964, ApJ, 140, 1467
- [70] Zwicky, F. 1966, ApJ, 143, 192